Rapid Communications

Stability of mobility edges in disordered interacting systems

Pietro Brighi,[1] Dmitry A. Abanin,[2] and Maksym Serbyn[1]
[1]*IST Austria, Am Campus 1, 3400 Klosterneuburg, Austria*
[2]*Department of Theoretical Physics, University of Geneva, 24 quai Ernest-Ansermet, 1211 Geneva, Switzerland*

(Received 18 May 2020; accepted 9 August 2020; published 26 August 2020)

Many-body localization provides a mechanism to avoid thermalization in isolated interacting quantum systems. The breakdown of thermalization may be complete, when all eigenstates in the many-body spectrum become localized, or partial, when the so-called many-body mobility edge separates localized and delocalized parts of the spectrum. Previously, De Roeck *et al.* [Phys. Rev. B **93**, 014203 (2016)] suggested a possible instability of the many-body mobility edge in energy density. The local ergodic regions—so-called "bubbles"—resonantly spread throughout the system, leading to delocalization. In order to study such instability mechanism, in this work we design a model featuring many-body mobility edge in *particle density*: the states at small particle density are localized, while increasing the density of particles leads to delocalization. Using numerical simulations with matrix product states, we demonstrate the stability of many-body localization with respect to small bubbles in large dilute systems for experimentally relevant timescales. In addition, we demonstrate that processes where the bubble spreads are favored over processes that lead to resonant tunneling, suggesting a possible mechanism behind the observed stability of many-body mobility edge. We conclude by proposing experiments to probe particle density mobility edge in the Bose-Hubbard model.

DOI: 10.1103/PhysRevB.102.060202

Introduction. Many-body localization (MBL) provides a mechanism to avoid thermalization in isolated quantum interacting systems [1,2]. Despite intensive theoretical [3,4] and experimental [5–11] studies, only fully MBL phase in one spatial dimension is relatively well understood. The fate of MBL in higher dimensions [12–16] and the possibility of the coexistence of localized and delocalized eigenstates in the same many-body spectrum [17] remain debated.

Similarly to the case of Anderson localization [18], the MBL and delocalized eigenstates cannot coexist at the same energy suggesting the existence of *many-body mobility edge (MBME)*—a certain energy in the spectrum separating localized and delocalized eigenstates [2]. In contrast to the noninteracting case, the energy of MBME scales *extensively* with system size. In the absence of a coupling to a bath, this leads to an exactly vanishing conductivity (in contrast to an exponentially small but finite value in Anderson insulator) until a certain critical temperature [2].

Recently De Roeck *et al.* [17] suggested a possible mechanism that may destroy MBME in large systems: a finite region with local energy density above the mobility edge—a "bubble"—may resonantly spread throughout the system thereby destroying localization everywhere. However, recent experiments [11] and matrix product state (MPS) simulations [19,20] gave evidence of MBME, at least on intermediate timescales. In addition, a number of numerical studies observed a mobility edge [21–25] using exact diagonalization (ED). Unfortunately, the ED is limited to relatively small system sizes; experiments with MBME in energy density are also challenging since they require energy resolution.

In order to overcome the above challenges, we propose to study MBME *in particle density*. This allows us to directly probe the mechanism of instability suggested in Ref. [17], which equally applies to MBME in any extensive conserved quantity. First, using numerical simulation with MPSs, we demonstrate that uniform dilute states remain localized even at system sizes of $L = 40$ sites up to 250 tunneling times (i.e., more than two orders of magnitude larger than the inverse local hopping). Next, we use a region with large particle density to reproduce the bubble described in [17] and track its influence on the dilute remainder of the system in a quantum quench. We do not find any evidence of resonant tunneling of the bubble, at least on experimentally relevant timescales.

In summary, the study of the particle density MBME facilitates the state preparation and analysis and allows us to access the dynamics of much larger systems using time evolution with MPS. We report the stability of the particle density mobility edge on long timescales and suggest that similar physics may be experimentally probed using the Bose-Hubbard model.

Correlated hopping model. We consider hard-core bosons on an open chain of size L, with the following Hamiltonian:

$$\hat{H} = t_1 \sum_{i=1}^{L-1} (c_{i+1}^{\dagger} c_i + \text{H.c.}) + \sum_{i=1}^{L} \epsilon_i \hat{n}_i + t_2 \sum_{i=2}^{L-1} (c_{i-1}^{\dagger} \hat{n}_i c_{i+1} + \text{H.c.}). \quad (1)$$

The first line corresponds to the noninteracting Anderson's model [26], where random on-site potential has a uniform distribution, $\epsilon_i \in [-W, W]$. The facilitated hopping in the second line enables motion of a *pair of particles* with amplitude t_2, $\bullet\bullet\circ \leftrightarrow \circ\bullet\bullet$, making the model interacting. The Hamiltonian (1)

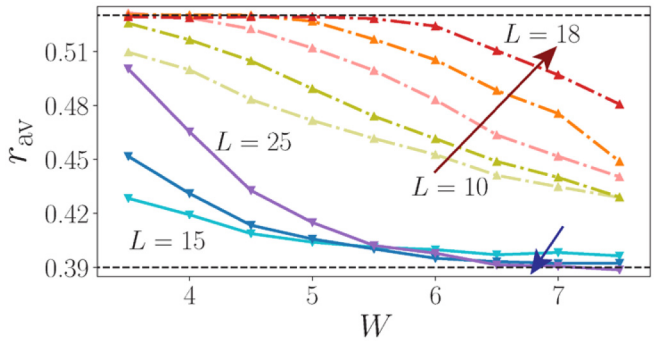

FIG. 1. Scaling of level spacing ratio demonstrates that at density $\nu = 1/5$ (solid lines, $L = 15, 20, 25$ with 3,4,5 particles) the system enters MBL phase for $W \geqslant 6.3$. In contrast, at half-filling $\nu = 1/2$ (dashed curves, $L = 10, \ldots, 18$) the critical disorder strength is much larger and in the entire range of disorder $r_{\rm av}$ approaches thermal value with increasing system size. Data is generated from ED/SI simulations with at least 10^3 disorder realizations using approximately 2% of eigenstates in the center of the spectrum.

has two channels for dynamics: the single-particle hopping prevails in dilute states, while the pair hopping is dominant at larger densities.

We note that a similar model was discussed in Ref. [17] in two dimensions, although only with two particles. The enhancement of localization length in the case of two interacting particles also received significant attention [27,28]. In a different direction, the fate of the single-particle mobility edge in the presence of interactions was studied [10,29]. In contrast, we study model (1) that does not have a single-particle mobility edge and consider the finite particle density regime.

We fix the value of the hopping parameters $t_1 = 0.5$ and $t_2 = 2$ so that the localization length of a single particle $\xi_{\rm SP} \lesssim 1$ and at the same time a single pair has a localization length $\xi_{\rm P} \gtrsim 2.5$ for $2.5 \lesssim W \lesssim 6$ [30]. For such a choice, our model does not suffer from finite size effects [31] and we establish MBME using eigenstate probes.

Eigenstate probes of localization. We use exact diagonalization and shift-invert (SI) numerical techniques to provide evidence for MBME in Hamiltonian (1). We analyze the average ratio of level spacings, $\delta_i = E_{i+1} - E_i$, in the middle of the spectrum, $r_{\rm av} = \langle \min(\delta_i, \delta_{i+1}) / \max(\delta_i, \delta_{i+1}) \rangle$. This is a commonly used probe of the MBL transition [22,32] that attains the value $r_{\rm P} \simeq 0.39$ for the Poisson level statistics, characteristic of the MBL phase, and $r_{\rm GOE} \simeq 0.53$ for the case of random Gaussian orthogonal ensemble (GOE), typical for chaotic Hamiltonians with time-reversal symmetry.

Figure 1 displays that at half-filling, $\nu = N/L = 1/2$, where N is the total number of particles and L is the chain length, the level statistics approaches GOE with increasing system size, which is consistent with the delocalized phase. In contrast, at $\nu = 1/5$ filling $r_{\rm av}$ flows towards $r_{\rm P}$ at strong disorder. In what follows we fix the disorder strength to be $W = 6.5$, since at this value the dilute limit is localized while the dense limit clearly flows towards delocalization. The scaling of entanglement entropy also confirms the coexistence of localized and delocalized phases for disorder $W = 6.5$ [30].

Quench dynamics. Having provided numerical evidence for the coexistence of localized and delocalized phases in small systems, we turn to quantum quench dynamics that distinguishes MBL from ergodic phase [5,33]. We consider quenches where the system is initially prepared in a product state and then evolved with the Hamiltonian (1). Starting with a density wave of period $1/\nu$, a configuration that contains no pairs, we calculate the density profile at late times. For the dilute case, $\nu = 1/5$, we use the time-evolved block decimation (TEBD) with MPS [34,35] (see [30] for additional details and benchmarks). This allows one to monitor the dynamics of systems as large as $L = 40$ sites up to times $T_{\rm max} = 500$. In the dense case ($\nu = 1/2$) we use ED and the Krylov subspace time evolution method. While ED allows one to access the infinite-time density profile, with the Krylov method, we simulate quantum dynamics up to $T_{\rm max} = 1000$.

The density profiles at late times look very different in the dense and dilute cases. While in the dilute case the system retains memory of the initial state [see Fig. 2(a)], at $\nu = 1/2$ quantum dynamics leads to a progressively more uniform density profile with increasing system size [Fig. 2(b)]. In order to quantify the difference in the form of the density profile at late times, in Fig. 2(c) we plot the average deviation of the density from the equilibrium thermal value ν, $\Delta n = (1/L) \sum_{i=1}^{L} |\langle \hat{n}_i(T_{\rm max}) \rangle - \nu|$. The deviation of late-time density from the thermal value, Δn, in the dense regime decays exponentially with the system size as $\Delta n \sim e^{-L/\xi_{\rm T}}$, where $\xi_{\rm T} \simeq 6.27$. In contrast, for the dilute case Δn shows no dependence on the system size, as is apparent in the density profiles. The characteristic length $\xi_{\rm T}$ extracted in the dense case gives the minimum size for genuine ergodic bubbles that can destroy the MBME according to Ref. [17].

Having confirmed the coexistence of localized and delocalized states at different values of particle density ν for the same disorder strength, we proceed with a more detailed study of the effect of a bubble, whose behavior is central to the mechanism proposed in [17]. Figure 2(d) illustrates the evolution of a nonuniform initial state, where a dense region represents the bubble. The bubble region consists of eight sites with two pairs of particles and has a local density of $\nu = 1/2$. The bubble is followed by a period-5 density wave that occupies $L - 10$ sites and two additional empty sites at the end of the chain. Although having $\nu = 8/30 > 1/5$, this state is still in a localized sector, as shown in [30]. The bubble leaks only weakly into the dilute region even at late times [see Fig. 2(d)], with particles far away from the bubble not being affected. In contrast, in the dense case, Fig. 2(g), the bubble with average density of $\nu = 2/3$ successfully melts the period-3 density wave state throughout the system.

Next, in panels Fig. 2(e) and 2(h) we further illustrate the differences between the density dynamics in the dense and dilute cases in the presence of a bubble. In both cases we plot the density of particles within subregions of small size k, $\tilde{\nu}_i = (1/k) \sum_{j=i}^{i+k-1} \langle n_j \rangle$, that are shown at the top of the plot. In the dilute case, Fig. 2(e), we observe that $\tilde{\nu}$ remains far from its thermal value even at late times, in contrast with [17], where an ergodic region larger than $\xi_{\rm T}$ is expected to delocalize the system. The densities of regions in the bubble and adjacent to the bubble seem to saturate, while the regions far away from the bubble show very slow dynamics. In contrast, the

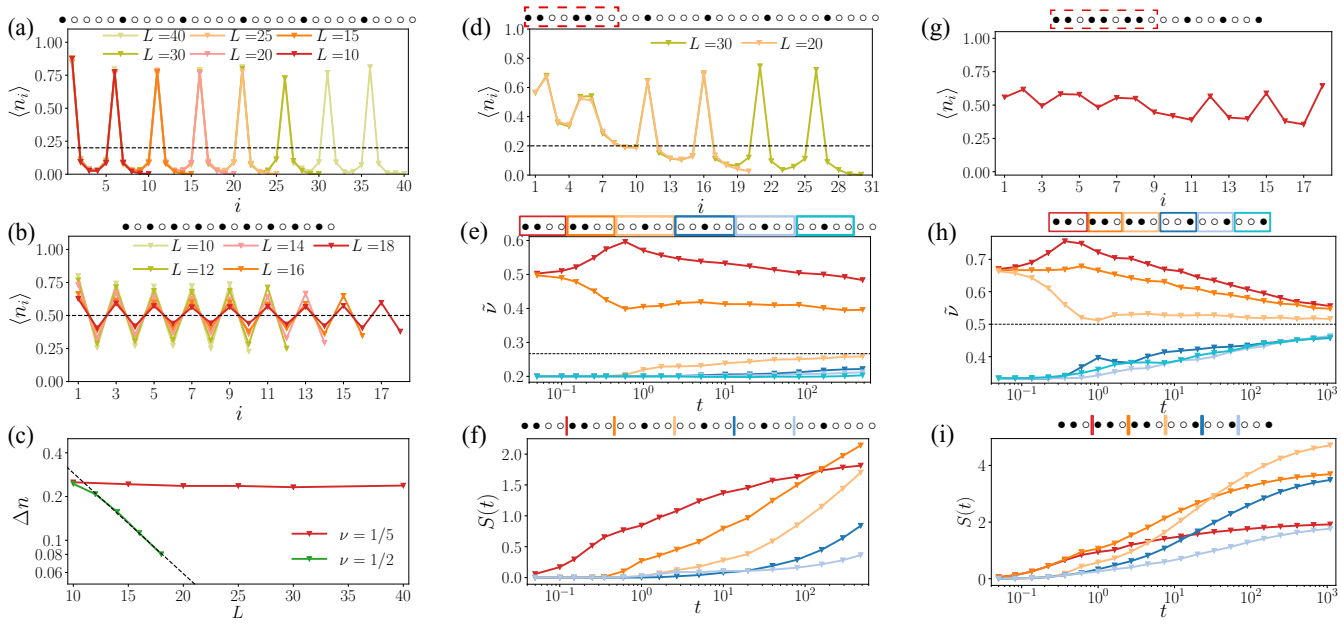

FIG. 2. (a)–(c) The quantum quench from the uniform density wave with period $1/\nu$ reveals memory of the initial state at $\nu = 1/5$ in (a), whereas in the dense case $\nu = 1/2$ (b) the charge pattern relaxes to zero exponentially in the system size as is shown in (c). (d)–(f) Stability of the dilute system against the bubble consisting of a half-filled region with four particles is illustrated in panel (d) by the density profile at $T_{\max}$. (e) The time dynamics of density in the coarse-grained regions (see the legend at the top) shows the absence of significant relaxation in regions away from the bubble. The density in the region at the boundary with the bubble increases logarithmically in time. (f) The onset of logarithmic entanglement dynamics after a transient is visible for all cuts (see the legend at the top) away from the bubble. (g)–(i) In contrast, the bubble delocalizes the system when the overall density $\nu = 1/2$. The residual density profile at $T_{\max} = 1000$ in panel (g) has only weak memory of the initial state. In addition, densities coarse-grained over three-site regions in (f) all tend to the equilibrium value of 1/2 and entanglement entropy in (i) displays faster than logarithmic growth for all cuts. The data are generated using TEBD and Krylov (ED) dynamics using between 5×10^4–100 (dilute) and 3×10^4–10^3 (dense) disorder realizations.

dense case, Fig. 2(h), shows that all expectation values evolve towards equilibrium, although the regions far away from the center of the chain display slow, logarithmic in time, growth of density.

Finally, we study the dynamics of the bipartite entanglement entropy, $S_{\rm vN}$ [see Figs. 2(f) and 2(i)]. The entanglement is defined as $S_{\rm vN} = -{\rm tr}\rho \ln \rho$, where ρ is the density matrix of the left subregion calculated from $|\psi(t)\rangle = e^{-i\hat{H}t}|\psi_0\rangle$. Different entanglement cuts shown at the top of Figs. 2(f) and 2(i) are encoded by their color. Consistent with MBL, the increase of entanglement in the region close to the bubble is logarithmic in time in Fig. 2(f) [36–39]. The entanglement across the cuts further away from the bubble begins to grow at significantly later times. For these more distant cuts, the initial uprise in entanglement corresponds to a slow logarithmic change of density [see Fig. 2(e)], and after saturation of density dynamics, we expect an onset of the logarithmic growth of entanglement. In contrast, the entanglement dynamics in Fig. 2(i) is always faster than logarithmic. In [30] we provide more details on the contribution of particle transport to entanglement [39,40], demonstrating that it is responsible for the logarithmic entanglement increase, in agreement with [41,42], whereas the configurational entanglement grows faster than logarithmic, and total entropy shows a power-law increase.

Bubble tunneling vs decay processes. The quench dynamics discussed above suggests that a bubble is not able to spread through the entire localized chain and remains in the vicinity of its initial position. At the same time, most of our quench simulations are restricted to finite, albeit long, times. In order to give complementary evidence for the bubble localization, we return to eigenstate properties that effectively probe the infinite time limit.

We start with an initial product state in the half-filled case illustrated for $L = 12$,

$$|\psi_1\rangle = \boxed{\bullet\bullet\circ\bullet\bullet\circ}\,\circ\circ\bullet\circ\circ\bullet, \tag{2}$$

that contains a bubble of $k = L/2$ sites with $\nu = 2/3$ filling (boxed region), followed by a sparser region with the same number of sites and density $\nu = 1/3$. To quantify the relation between the probability of the bubble tunneling to the opposite end of the system and the probability of the bubble spreading throughout the system, we use a spatial reflection of $|\psi_1\rangle$ and uniform density wave as a representative of the state with bubble tunneling and spreading, respectively:

$$|\psi_2^t\rangle = \bullet\circ\circ\bullet\circ\circ\,\boxed{\circ\bullet\bullet\circ\bullet\bullet}, \tag{3}$$

$$|\psi_2^s\rangle = \bullet\circ\bullet\circ\bullet\circ\bullet\circ\bullet\circ\bullet\circ\bullet, \tag{4}$$

illustrated for $L = 12$ and $\nu = 1/2$ filling. For dilute configurations at $\nu = 1/5$ we define the bubble as a region of size $2(\nu L - 1)$ with density 1/2, joined with a dilute remainder. For $L = 20$ such a state is

$$|\psi_1\rangle = \boxed{\bullet\bullet\circ\bullet\circ\circ}\,\circ\circ\circ\circ\circ\circ\bullet\circ\circ\circ\circ\circ\circ\circ\circ.$$

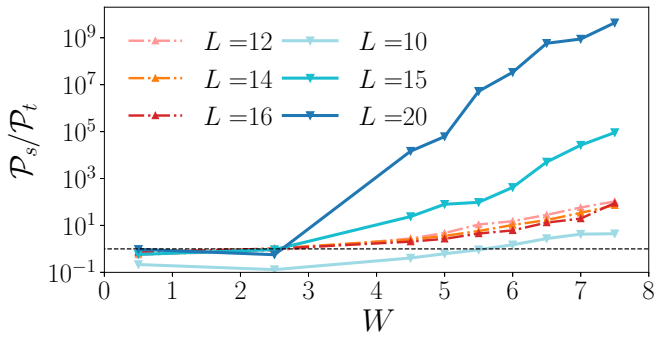

FIG. 3. The rapid increase of the ratio of $\mathcal{P}_s/\mathcal{P}_t$ with system size and disorder strength reveals that in the dilute case, $\nu = 1/5$, the probability for bubble spreading is strongly enhanced compared to the probability of bubble tunneling to the opposite end of the system. For the dense case these two probabilities are of the same order and approach each other with increasing system size in a broad range of disorders. Averaging is done over at least 2.5×10^3 disorder realizations.

It is straightforward to show that the infinite-time average probability of finding the system with the wave function $e^{-i\hat{H}t}|\psi_1\rangle$ in the product state $|\psi_2\rangle$ is given by

$$\mathcal{P}(|\psi_1\rangle, |\psi_2\rangle) = \sum_{\alpha=1}^{\mathcal{N}} |\langle E_\alpha|\psi_1\rangle\langle E_\alpha|\psi_2\rangle|^2, \tag{5}$$

where $|E_\alpha\rangle$ are the complete set of eigenstates of $\hat{H}$. Equation (5) quantifies the similarity in the expansion of two different states $|\psi_{1,2}\rangle$ over the basis $|E_\alpha\rangle$ and reduces to the conventional participation ratio when $|\psi_1\rangle = |\psi_2\rangle$.

In order to reveal the relation between bubble decay and tunneling processes, we calculate the ratio of probabilities of bubble decaying, $\mathcal{P}_s = \mathcal{P}(|\psi_1\rangle, |\psi_2^s\rangle)$, with $|\psi_2^s\rangle$ from Eq. (4), to bubble tunneling, $\mathcal{P}_t = \mathcal{P}(|\psi_1\rangle, |\psi_2^t\rangle)$ with $|\psi_2^t\rangle$ from Eq. (3). In the dense case, these two probabilities are of the same order and moreover tend to identity with increasing system size as expected in the delocalized phase (see Fig. 3). In the dilute case, the ratio $\mathcal{P}_s/\mathcal{P}_t$ is rapidly increasing with both disorder and system size. This proves that the bubble tunneling processes are strongly suppressed compared to the processes where the bubble spreads throughout the system, calling into question the applicability of the resonance argument of [17].

Experimental realization. Finally, we discuss a possible way to observe the physics related to MBME in experiments with ultracold atoms. Within the disordered Aubry-André bosonic Hamiltonian,

$$\hat{H} = \sum_i [t(a_i^\dagger a_{i+1} + \text{H.c.}) + \epsilon_i n_{i,\sigma} + U n_i(n_i - 1)], \tag{6}$$

that is actively used to study MBL physics [39,43], the bubbles can be represented by regions with $\langle a_i^\dagger a_i\rangle = \rho > 1$ bosons per site. A particle within such region has a hopping matrix element enhanced by the Bose factor of $\langle\rho\rangle$, thus playing the role of hopping t_2 in model (1). In the regime of densities and disorder strengths such that the enhanced hopping $\langle\rho\rangle t$ corresponds to localization lengths significantly larger than lattice spacing, $\xi_{\text{dense}} > a$, whereas a single boson localization length is $\xi \lesssim a$, this model will implement similar physics to our toy model. Note that at the same time it is important to keep interaction U low enough, $U \leqslant t$, to avoid the formation of minibands related to long-lived doublons.

By initializing the system in a product state with a dense region of bosons in the center of the trap along with low density of bosons away from such a region, the dynamics under Hamiltonian (6) will probe the ability of the bubble to melt the imbalance [5] away from its original position. From our simulations we expect the absence of imbalance relaxation far away from the bubble. In a different direction, doublons [44,45] or second species of particles not subject to disorder [9] are also promising candidates that can play a role of the bubble.

Discussion. We presented a model with MBME in particle density and investigated its properties numerically using ED and time evolution with MPS. We find strong evidence of the persistence of localization at infinite times for small systems and also observe memory of initial configuration until times of $T_{\max} = 500$ for systems with up to $L = 40$ sites. These times are at least two orders of magnitude larger compared to the inverse local hopping, $\hbar/t_1$, and are achievable with cold-atom experiments. While we cannot rule out a residual very slow delocalization at much later times, the constructed model allows us to bound the timescale up to which the localization remains stable in very large systems that are beyond the reach for ED.

The model with MBME in particle density presented in this work allows for direct tests of the arguments about the instability of MBME [17]. In order for the bubble to move throughout the system it is important that the bubble does not disappear by spreading and that configurations with bubbles situated at different locations are effectively coupled to each other. Our simulations reveal that dilute systems have no trace of bubble reemerging at a different location within the system. Moreover, even the expectation value of the pair density $\langle n_i n_{i+1}\rangle$ (pairs are building blocks of the bubble) is exponentially suppressed away from the original location of the dense bubble [30]. In an alternative approach, we directly test the probability of the bubble to emerge at the opposite end of the system at infinite time and find it to be strongly suppressed.

To conclude, we expect that the proposed model will enable further investigations of particle density MBME. Studies of the structure of matrix elements, extension of the theory of local integrals of motion (LIOMs) [46,47] to systems with MBME in particle density [23], and studies of the effect of a small bath on a localized system [48–51] using our model represent promising avenues for future work.

Acknowledgments. We acknowledge useful discussions with W. De Roeck and A. Michailidis. P.B. was supported by the European Union's Horizon 2020 research and innovation program under the Marie Sklodowska-Curie Grant Agreement No. 665385. D.A. was supported by the Swiss National Science Foundation. M.S. was supported by European Research Council (ERC) under the European Union's Horizon 2020 research and innovation program (Grant

Agreement No. 850899). This work benefited from visits to KITP, supported by the National Science Foundation under Grant No. NSF PHY-1748958 and from the program "Thermalization, Many Body Localization and Hydrodynamics" at International Centre for Theoretical Sciences (Code: ICTS/hydrodynamics2019/11).

[1] L. Fleishman and P. W. Anderson, Interactions and the Anderson transition, Phys. Rev. B **21**, 2366 (1980).
[2] D. M. Basko, I. L. Aleiner, and B. L. Altshuler, Metal–insulator transition in a weakly interacting many-electron system with localized single-particle states, Ann. Phys. **321**, 1126 (2006).
[3] D. A. Abanin, E. Altman, I. Bloch, and M. Serbyn, "Colloquium: Many-body localization, thermalization, and entanglement," Rev. Mod. Phys. **91**, 021001 (2019).
[4] R. Nandkishore and D. A. Huse, Many-body localization and thermalization in quantum statistical mechanics, Annu. Rev. Condens. Matter Phys. **6**, 15 (2015).
[5] M. Schreiber, S. S. Hodgman, P. Bordia, H. P. Lüschen, M. H. Fischer, R. Vosk, E. Altman, U. Schneider, and I. Bloch, Observation of many-body localization of interacting fermions in a quasirandom optical lattice, Science **349**, 842 (2015).
[6] P. Bordia, H. P. Lüschen, S. S. Hodgman, M. Schreiber, I. Bloch, and U. Schneider, Coupling Identical One-Dimensional Many-Body Localized Systems, Phys. Rev. Lett. **116**, 140401 (2016).
[7] J. Choy, S. Hild, J. Zeiher, P. Schauß, A. Rubio-Abadal, T. Yefsah, V. Khemani, D. A. Huse, I. Bloch, and C. Gross, Exploring the many-body localization transition in two dimensions, Science **352**, 1547 (2016).
[8] B. Chiaro *et al.*, Direct measurement of non-local interactions in the many-body localized phase, arXiv:1910.06024.
[9] A. Rubio-Abadal, J.-Y. Choi, J. Zeiher, S. Hollerith, J. Rui, I. Bloch, and C. Gross, Many-Body Delocalization in the Presence of a Quantum Bath, Phys. Rev. X **9**, 041014 (2019).
[10] T. Kohlert, S. Scherg, X. Li, H. P. Lüschen, S. Das Sarma, I. Bloch, and M. Aidelsburger, Observation of Many-Body Localization in a One-Dimensional System with a Single-Particle Mobility Edge, Phys. Rev. Lett. **122**, 170403 (2019).
[11] Q. Guo, C. Cheng, Z.-H. Sun, Z. Song, H. Li, Z. Wang, W. Ren, H. Dong, D. Zheng, Y.-R. Zhang, R. Mondaini, H. Fan, and H. Wang, Observation of energy resolved many-body localization, arXiv:1912.02818.
[12] W. De Roeck and F. Huveneers, Stability and instability towards delocalization in many-body localization systems, Phys. Rev. B **95**, 155129 (2017).
[13] T. B. Wahl, A. Pal, and S. H. Simon, Signatures of the many-body localized regime in two dimensions, Nat. Phys. **15**, 164 (2019).
[14] I.-D. Potirniche, S. Banerjee, and E. Altman, Exploration of the stability of many-body localization in $d > 1$, Phys. Rev. B **99**, 205149 (2019).
[15] A. Kshetrimayum, M. Goihl, and J. Eisert, Time evolution of many-body localized systems in two spatial dimensions, arXiv:1910.11359.
[16] Elmer V. H. Doggen, I. V. Gornyi, A. D. Mirlin, and D. G. Polyakov, Slow many-body delocalization beyond one dimension, arXiv:2002.07635.
[17] W. De Roeck, F. Huveneers, M. Müller, and M. Schiulaz, Absence of many-body mobility edges, Phys. Rev. B **93**, 014203 (2016).
[18] N. F. Mott, Electrons in disordered structures, Adv. Phys. **16**, 49 (1967).
[19] T. Chanda, P. Sierant, and J. Zakrzewski, Many-body localization transition in large quantum spin chains: The mobility edge, arXiv:2006.02860.
[20] E. V. H. Doggen, F. Schindler, K. S. Tikhonov, A. D. Mirlin, T. Neupert, D. G. Polyakov, and I. V. Gornyi, Many-body localization and delocalization in large quantum chains, Phys. Rev. B **98**, 174202 (2018).
[21] M. Serbyn, Z. Papić, and D. A. Abanin, Criterion for Many-Body Localization-Delocalization Phase Transition, Phys. Rev. X **5**, 041047 (2015).
[22] D. J. Luitz, N. Laflorencie, and F. Alet, Many-body localization edge in the random-field Heisenberg chain, Phys. Rev. B **91**, 081103 (2015).
[23] S. D. Geraedts, R. N. Bhatt, and R. Nandkishore, Emergent local integrals of motion without a complete set of localized eigenstates, Phys. Rev. B **95**, 064204 (2017).
[24] M. Goihl, J. Eisert, and C. Krumnow, Exploration of the stability of many-body localized systems in the presence of a small bath, Phys. Rev. B **99**, 195145 (2019).
[25] R. Yao and J. Zakrzewski, Many-body localization in the Bose-Hubbard model: Evidence for mobility edge, Phys. Rev. B **102**, 014310 (2020).
[26] P. W. Anderson, Absence of diffusion in certain random lattices, Phys. Rev. **109**, 1492 (1958).
[27] D. L. Shepelyansky, Coherent Propagation of Two Interacting Particles in a Random Potential, Phys. Rev. Lett. **73**, 2607 (1994).
[28] Y. Imry, Coherent propagation of two interacting particles in a random potential, Europhys. Lett. **30**, 405 (1995).
[29] X. Li, S. Ganeshan, J. H. Pixley, and S. Das Sarma, Many-Body Localization and Quantum Nonergodicity in a Model with a Single-Particle Mobility Edge, Phys. Rev. Lett. **115**, 186601 (2015).
[30] See Supplemental Material at http://link.aps.org/supplemental/10.1103/PhysRevB.102.060202 for motivation for the choice of parameters, additional evidence of MBME, benchmarks of the MPS simulations and further comparison of the processes where bubble decays or tunnels without any decay.
[31] Z. Papić, E. M. Stoudenmire, and D. A. Abanin, Many-body localization in disorder-free systems: The importance of finite-size constraints, Ann. Phys. **362**, 714 (2015).
[32] A. Pal and D. A. Huse, Many-body localization phase transition, Phys. Rev. B **82**, 174411 (2010).
[33] M. Serbyn, Z. Papić, and D. A. Abanin, Quantum quenches in the many-body localized phase, Phys. Rev. B **90**, 174302 (2014).

[34] Guifré Vidal, Efficient Classical Simulation of Slightly Entangled Quantum Computations, Phys. Rev. Lett. **91**, 147902 (2003).
[35] ITensor Library (version 3.1.1), http://itensor.org.
[36] M. Znidaric, T. Prosen, and P. Prelovsek, Many-body localization in the Heisenberg *xxz* magnet in a random field, Phys. Rev. B **77**, 064426 (2008).
[37] J. H. Bardarson, F. Pollmann, and J. E. Moore, Unbounded Growth of Entanglement in Models of Many-Body Localization, Phys. Rev. Lett. **109**, 017202 (2012).
[38] M. Serbyn, Z. Papić, and D. A. Abanin, Universal Slow Growth of Entanglement in Interacting Strongly Disordered Systems, Phys. Rev. Lett. **110**, 260601 (2013).
[39] A. Lukin, M. Rispoli, R. Schittko, M. E. Tai, A. M. Kaufman, S. Choi, V. Khemani, J. Léonard, and M. Greiner, Probing entanglement in a many-body–localized system, Science **364**, 256 (2019).
[40] R. Islam, R. Ma, P. M. Preiss, M. E. Tai, A. Lukin, M. Rispoli, and M. Greiner, Measuring entanglement entropy in a quantum many-body system, Nature (London) **528**, 77 (2015).
[41] M. Kiefer-Emmanouilidis, R. Unanyan, M. Fleischauer, and J. Sirker, Evidence for Unbounded Growth of the Number Entropy in Many-Body Localized Phases, Phys. Rev. Lett. **124**, 243601 (2020).
[42] D. J. Luitz, and Y. Bar Lev, Is there slow particle transport in the MBL phase? arXiv:2007.13767.
[43] M. Rispoli, A. Lukin, R. Schittko, S. Kim, M. E. Tai, J. Léonard, and M. Greiner, Quantum critical behaviour at the many-body localization transition, Nature (London) **573**, 385 (2019).
[44] U. Krause, T. Pellegrin, P. W. Brouwer, D. A. Abanin, and M. Filippone, Nucleation of ergodicity by a single mobile impurity in supercooled insulators, arXiv:1911.11711.
[45] M. Schecter, T. Iadecola, and S. Das Sarma, Configuration-controlled many-body localization and the mobility emulsion, Phys. Rev. B **98**, 174201 (2018).
[46] M. Serbyn, Z. Papić, and D. A. Abanin, Local Conservation Laws and the Structure of the Many-Body Localized States, Phys. Rev. Lett. **111**, 127201 (2013).
[47] D. A. Huse, R. Nandkishore, and V. Oganesyan, Phenomenology of fully many-body-localized systems, Phys. Rev. B **90**, 174202 (2014).
[48] R. Nandkishore, Many-body localization proximity effect, Phys. Rev. B **92**, 245141 (2015).
[49] D. J. Luitz, F. Huveneers, and W. De Roeck, How a Small Quantum Bath can Thermalize Long Localized Chains, Phys. Rev. Lett. **119**, 150602 (2017).
[50] K. Hyatt, J. R. Garrison, A. C. Potter, and B. Bauer, Many-body localization in the presence of a small bath, Phys. Rev. B **95**, 035132 (2017).
[51] P. J. D. Crowley and A. Chandran, Avalanche induced coexisting localised and thermal regions in disordered chains, arXiv:1910.10812.